Correlation potentials for molecular bond dissociation within the self-consistent random phase approximation

Maria Hellgren,[1,a)] Daniel R. Rohr,[1,2] and E. K. U. Gross[1]

[1]*Max-Planck-Institut für Mikrostrukturphysik, Weinberg 2, 06120 Halle (Saale), Germany*
[2]*Fritz-Haber-Institut der Max-Planck-Gesellschaft, Faradayweg 2-4, 14195 Berlin, Germany*

Self-consistent correlation potentials for H_2 and LiH for various inter-atomic separations are obtained within the random phase approximation (RPA) of density functional theory. The RPA correlation potential shows a peak at the bond midpoint, which is an exact feature of the true correlation potential, but lacks another exact feature: the step important to preserve integer charge on the atomic fragments in the dissociation limit. An analysis of the RPA energy functional in terms of fractional charge is given which confirms these observations. We find that the RPA misses the derivative discontinuity at odd integer particle numbers but explicitly eliminates the fractional spin error in the exact-exchange functional. The latter finding explains the improved total energy in the dissociation limit. © *2012 American Institute of Physics*. [doi:10.1063/1.3676174]

I. INTRODUCTION

The random phase approximation (RPA) in Kohn-Sham (KS) density functional theory (DFT) has in recent years received considerable attention in quantum chemistry[1–3] and material science.[4–11] The RPA incorporates exchange effects exactly and the correlation energy is treated nonperturbatively by summing a subset of polarization diagrams to infinite order.[12,13] Furthermore, the RPA can be systematically improved being the first approximation within the so-called adiabatic connection fluctuation dissipation (ACFD) framework.[14–16]

The RPA is an implicit functional of the density and can therefore include non-local correlation effects, e.g., the van der Waals interactions. That these are, indeed, accurately captured by the RPA has been demonstrated in many recent works.[17–19] For systems described by strong Hubbard-like correlations, the RPA is, however, still not fully investigated. A popular test case in this regard is the dissociation of diatomic molecules with covalent bonds.[20] All density functional approximations constructed so far fail in this context, if proper spin-symmetry is enforced. The total energy in the dissociation limit is too high and spurious fractional charges are found at the fragments.

The large error in the total energy has been characterized as static correlation error or so-called fractional spin error, studied in detail in the pioneering works of Cohen, Mori-Sànchez, and Yang.[21–23] It has been demonstrated that the RPA strongly improves the dissociation limit for homoatomic systems such as the H_2 molecule.[24–27]

Spurious fractional charges, on the other hand, appear only in the dissociation limit of heteroatomic molecules and are related to an incorrect behavior of the total energy as a function of particle number. The exact energy functional exhibits a kink or derivative discontinuity at integer particle numbers along with a straight line behavior between the integers.[28] The smooth and nonlinear behavior of approximate functionals leads to charged fragments in the dissociation limit, meaning that one electron is too delocalized, i.e., spread over both fragments. This error is known in the literature as delocalization error or fractional charge error.[22,23,29] The delocalization error of the RPA has been studied only for the dissociation of open-shell H_2^+ and He_2^+.[30] It was found to be rather severe leading to too low total energies. Whether the RPA suffers from fractional charge error in the cases of heteronuclear molecules is presently unknown.

The exact functional ensures neutral dissociation fragments by virtue of the KS potential.[31–33] In the dissociation limit, the highest occupied orbital of each of the fragments must be aligned (or degenerate). Consequently, the highest occupied molecular orbital (HOMO) of the whole system (including both fragments) is a linear combination of the orbitals of each fragment. To obtain equal weights, i.e., integer charge, at the fragments the KS potential exhibits a sharp step at the bond midpoint, shifting the energy levels of only one of the fragments. This feature is a direct consequence of the derivative discontinuity in the correlation part of the energy.[34,35] Another feature of the exact KS correlation potential of dissociated molecules is a peak at the bond midpoint.[36] The peak emerges with increasing inter-atomic distance, and acts to further localize the electrons.

The RPA correlation potential for atoms was recently obtained[37,38] and showed a close resemblance to the exact correlation potential. However, all RPA calculations on molecules have so far been carried out using potentials originating from other functionals and hence precluding a full assessment of the RPA. The aim of this work is to provide a more complete analysis of the RPA. To this purpose, we have calculated self-consistent RPA potentials for molecules and investigated the RPA correlation potentials for H_2 and LiH at different inter-atomic distances. These systems allow us to study both the static correlation error and the delocalization error. Moreover, the LiH is an example where a self-consistent calculation is essential. We have also analyzed the RPA

---

a)Author to whom correspondence should be addressed. Electronic mail: hellgren@mpi-halle.de.

    136, 034106-1

energy functional in terms of fractional charge by studying the RPA functional on an extended domain of spin-compensated densities allowing for non-integer number of particles.

We conclude that the RPA potentials exhibit the peak at the bond midpoint but lack the step feature, where the latter is related to a missing intra-shell derivative discontinuity. The total energy of LiH is, however, still largely improved in the dissociation limit as compared to, e.g., the exact-exchange (EXX) functional, suggesting only a smaller delocalization error.

II. RPA CORRELATION ENERGY AND POTENTIAL

Within the ACFD framework the exact correlation energy is written as[39–41]

$$E_c = \frac{i}{2} \int_0^1 d\lambda \int_{-\infty}^{\infty} \frac{d\omega}{2\pi} \, \text{Tr} \{ v[\chi_\lambda(\omega) - \chi_s(\omega)] \}, \quad (1)$$

where χ_s is the non-interacting KS density response function and χ_λ is the scaled interacting density response function. The scaling refers to a system with a linearly scaled Coulomb interaction $\lambda v(\mathbf{r}, \mathbf{r}')$ plus a fictitious potential which keeps the density fixed as λ is changed. The parameter λ runs between 0 (non-interacting KS case) and 1 (fully interacting case). We have used the shorthand notation $\text{Tr} \, fg = \int d\mathbf{r} d\mathbf{r}' f(\mathbf{r}, \mathbf{r}') g(\mathbf{r}', \mathbf{r})$ for any two-point functions f and g. Within TDDFT, the function χ^λ reads[42]

$$\chi_\lambda = \chi_s + \chi_s \left[\lambda v + f_{xc}^\lambda \right] \chi_\lambda. \quad (2)$$

The scaled XC kernel f_{xc}^λ is defined as the functional derivative of the scaled XC potential v_{xc}^λ with respect to the density n, evaluated at the ground state density.

In the RPA, $f_{xc}^\lambda = 0$ and thus corresponds to the simplest approximation within the ACFD formalism. Within the RPA, the λ-integral in Eq. (1) can be evaluated analytically with the result

$$E_c = -\frac{i}{2} \int \frac{d\omega}{2\pi} \, \text{Tr} \{ \ln[1 - v\chi_s] + v\chi_s \}. \quad (3)$$

Diagrammatically, Eq. (3) is equal to an infinite summation of ring-diagrams.

The RPA correlation potential v_c can be obtained as the functional derivative of Eq. (3) with respect to the density. If we let V_s signify the total KS potential, G_s the non-interacting KS Green function, and $\chi_s = -iG_sG_s$, the functional derivative can be obtained via the chain rule

$$n_c \equiv \frac{\delta E_c}{\delta n} \frac{\delta n}{\delta V_s} = \frac{\delta E_c}{\delta G_s} \frac{\delta G_s}{\delta V_s}. \quad (4)$$

The result is the well-known linearized Sham-Schlüter equation,[43,44]

$$\int \chi_s(1, 2) v_c(2) d2 = \int \Lambda(3, 2; 1) \Sigma_c(2, 3) d2 d3. \quad (5)$$

Here, we have used the notation $(\mathbf{r}_1, t_1) = 1$, etc. and introduced $\Lambda(3, 2; 1) = -iG_s(3, 1)G_s(1, 2)$. The correlation part of the self-energy Σ_c in the RPA is given by

$$\Sigma_c = i \frac{\delta E_c}{\delta G_s} = iv\chi^{\text{RPA}} vG_s, \quad (6)$$

where

$$\chi^{\text{RPA}} = \chi_s + \chi_s v \chi^{\text{RPA}}. \quad (7)$$

In the Appendix, we show the expression for n_c, i.e., the right-hand side of Eq. (5), in terms of KS orbitals and KS eigenvalues.

III. FRACTIONAL CHARGE AND SPIN

The RPA functional produces accurate dissociation energies for H_2, in contrast to all common density functionals which yield a far too high energy due to a spurious self-interaction in the H fragments. It is well known that EXX is self-interaction free in the case of a spin-polarized H atom. In the dissociation limit of H_2, the H atoms are, however, not spin-polarized, but rather described by a mixture of a spin-up and a spin-down H atom, in which case EXX does suffer from self-interaction. To obtain the correct dissociation limit, a significant correlation contribution is thus needed. In the following, we will show that the RPA correlation functional exactly cancels the error in the EXX functional in the dissociation limit. The total energy will still not be exact as the correlation energy contains a self-correlation term, which does not vanish in the dissociation limit.

A. RPA in the dissociation limit

The RPA energy is an explicit functional of the KS Green function G_s and for spin-compensated systems, G_s is proportional to the identity matrix in spin-space. In the frequency domain, a spin-component of G_s reads

$$G_s(\mathbf{r}, \mathbf{r}', \omega) = \sum_k^{\text{occ}} G_k^-(\mathbf{r}, \mathbf{r}', \omega) + \sum_k^{\text{uocc}} G_k^+(\mathbf{r}, \mathbf{r}', \omega), \quad (8)$$

where we have defined

$$G_k^{\pm}(\mathbf{r}, \mathbf{r}', \omega) = \frac{\varphi_k(\mathbf{r})\varphi_k(\mathbf{r}')}{\omega - \varepsilon_k \pm i\eta}, \quad (9)$$

with φ_k being a KS spin-orbital and ε_k the corresponding eigenvalue. Consider now a stretched homonuclear diatomic molecule composed of atoms A and B. For large but finite inter-atomic separation R, the molecular KS orbitals can approximately be written as symmetric and anti-symmetric linear combination of the atomic KS orbitals,

$$\varphi_k(\mathbf{r}) = \frac{1}{\sqrt{2}} \left[\varphi_k^A(\mathbf{r}) \pm \varphi_k^B(\mathbf{r}) \right], \quad (10)$$

where $\varphi_k^A(\mathbf{r})$ is a KS orbital of atom A. This expression becomes exact as $R \rightarrow \infty$. It is easy to show that in the dissociation limit

$$E^{\text{RPA}}[G_s] \rightarrow E^{\text{RPA}}[G_s^A] + E^{\text{RPA}}[G_s^B], \quad (11)$$

where

$$G_s^A = \sum_{k \neq 0}^{\text{occ}} G_k^- + \sum_{k \neq 0}^{\text{uocc}} G_k^+ + \frac{1}{2} \left[G_0^+ + G_0^- \right]. \quad (12)$$

Here, G_s^A contains only states of the isolated atom A. The orbital $k = 0$ is the special orbital of the highest occupied state

which has to be considered partially occupied and partially unoccupied. For a homoatomic system, the fraction is always 1/2.

In the case of a covalent bonded heteronuclear diatomic molecule, a similar analysis can be carried out. The only difference is that now only the highest occupied and lowest unoccupied arise from a degeneracy of the isolated atoms. Due to the lack of symmetry, we also have to allow for a more general linear combination of KS orbitals,

$$\varphi_0^{\text{LUMO}}(\mathbf{r}) = \frac{1}{\sqrt{2}}\left[\sqrt{p}\varphi_0^A(\mathbf{r}) - \sqrt{(2-p)}\varphi_0^B(\mathbf{r})\right], \quad (13)$$

$$\varphi_0^{\text{HOMO}}(\mathbf{r}) = \frac{1}{\sqrt{2}}\left[\sqrt{(2-p)}\varphi_0^A(\mathbf{r}) + \sqrt{p}\varphi_0^B(\mathbf{r})\right], \quad (14)$$

where $p \in [0, 2]$. The KS Green functions to be inserted in Eq. (11) become

$$G_s^A = \sum_{k \neq 0}^{\text{occ}} G_k^- + \sum_{k \neq 0}^{\text{uocc}} G_k^+ + \frac{p}{2}G_0^+ + \frac{2-p}{2}G_0^-, \quad (15)$$

$$G_s^B = \sum_{k \neq 0}^{\text{occ}} G_k^- + \sum_{k \neq 0}^{\text{uocc}} G_k^+ + \frac{2-p}{2}G_0^+ + \frac{p}{2}G_0^-. \quad (16)$$

In the exact system, the energy assumes its minimum at $p = 1$. This is, however, not guaranteed using an approximate functional. In fact, most functionals yield a so-called fractional charge error on the atomic fragments (i.e., the minimum is found at $p \neq 1$).

B. Fractional charge

In this section, we derive an expression for the RPA correlation energy in terms of fractionally charged spin-compensated systems. To this end, we consider ensembles of the following form:

$$\hat{\gamma}^< = (1-p)|0\rangle\langle 0| + \frac{p}{2}(|\uparrow\rangle\langle\uparrow| + |\downarrow\rangle\langle\downarrow|) \quad (17)$$

for $p \in [0, 1)$,

$$\hat{\gamma}^> = \frac{2-p}{2}(|\uparrow\rangle\langle\uparrow| + |\downarrow\rangle\langle\downarrow|) + (p-1)|\uparrow\downarrow\rangle\langle\uparrow\downarrow|$$

for $p \in (1, 2]$, \quad (18)

where $|0\rangle$ refers to the ground state of N_0 even number of electrons, $|\uparrow\downarrow\rangle$ refers to a spin-compensated $(N_0 + 2)$-state, and $|\downarrow\rangle(|\uparrow\rangle)$ a spin-down(up) polarized state with $N_0 + 1$ electrons. The definition of the non-interacting spin-up $G_\alpha^\uparrow$ and spin-down $G_\alpha^\downarrow$ Green functions are

$$G_\alpha^\uparrow(\mathbf{r}t, \mathbf{r}'t') = \langle\alpha|T\{\psi^\uparrow(\mathbf{r}t)\psi^\uparrow(\mathbf{r}'t')^\dagger\}|\alpha\rangle, \quad (19)$$

$$G_\alpha^\downarrow(\mathbf{r}t, \mathbf{r}'t') = \langle\alpha|T\{\psi^\downarrow(\mathbf{r}t)\psi^\downarrow(\mathbf{r}'t')^\dagger\}|\alpha\rangle, \quad (20)$$

where α can be any of the states $|0\rangle$, $|\downarrow\rangle$, $|\uparrow\rangle$, or $|\uparrow\downarrow\rangle$ in the KS system. Here, T is the time-ordering operator and $\psi^\beta(\mathbf{r}t)$ is the field operator with the property of adding $\psi^\beta(\mathbf{r}t)^\dagger$ or

removing $\psi^\beta(\mathbf{r}t)$ an electron with spin β in $\mathbf{r}$ at time t. Evaluating the Green functions as ensemble expectation values using Eqs. (17) and (18) we find Green functions exactly of the form as in Eqs. (15) and (16). Thus, the ensembles proposed correspond to how an atom in the RPA is described in the dissociation limit.

The RPA correlation energy is usually evaluated using the time-ordered KS response function χ_s. Using the ensemble Green functions, we find

$$\chi_s^E(\mathbf{r}, \mathbf{r}', \omega) = -i\pi\delta(\omega)p(2-p)|\varphi_0(\mathbf{r})|^2|\varphi_0(\mathbf{r}')|^2 + \tilde{\chi}_s^p(\mathbf{r}, \mathbf{r}', \omega), \quad (21)$$

where

$$\tilde{\chi}_s^p(\mathbf{r}, \mathbf{r}', \omega) = 2\sum_q \frac{f_q(\mathbf{r})f_q(\mathbf{r}')}{\omega - \varepsilon_q + 2i\eta} - \frac{f_q(\mathbf{r})f_q(\mathbf{r}')}{\omega + \varepsilon_q - 2i\eta}, \quad (22)$$

and we have performed a spin summation. The orbitals φ_k are now referring to the orbitals of an isolated atom. The index $q = (k, k')$ is a composite index of occupied (k) and unoccupied (k') states. The special transition $q = (0, 0)$ is excluded since it has been taken out explicitly (first term in Eq. (21)). The functions $f_q(\mathbf{r}) = \varphi_k(\mathbf{r})\varphi_{k'}(\mathbf{r})$ are called excitation functions and we note that when φ_0 is occupied it should be multiplied by $\sqrt{p/2}$ and when it is unoccupied it should be multiplied by $\sqrt{(2-p)/2}$. When calculating the correlation energy, the interacting RPA response function has to first be evaluated $\chi_\lambda^E = \chi_s^E + \lambda\chi_s^E v \chi_\lambda^E$. The final expression of the RPA correlation energy reads

$$E_c = -\frac{p(2-p)}{4}\int d\mathbf{r}d\mathbf{r}'|\varphi_0(\mathbf{r})|^2 v(\mathbf{r}, \mathbf{r}')|\varphi_0(\mathbf{r}')|^2$$

$$+ \frac{i}{2}\int_0^1 d\lambda \int_{-\infty}^\infty \frac{d\omega}{2\pi}\text{Tr}\left\{v\left[\tilde{\chi}_\lambda^p(\omega) - \tilde{\chi}_s^p(\omega)\right]\right\}, \quad (23)$$

where $\tilde{\chi}_\lambda^p(\omega)$ is the scaled interacting response function calculated using Eq. (22). This equation will allow us to investigate the fractional spin error in Sec. III C and to obtain numerical results for the fractional charge error in Sec. V.

C. Fractional spin error

The fractional spin error is defined as the energy difference of a system with $N_0 + 1$ electrons with one electron spin polarized (sp) on one hand, and the same system but fully spin compensated (sc) on the other hand. Let us split the RPA interaction energy into the sum of Hartree and exchange energy (Hx) and the correlation energy. The sum of Hx energy in the sp case reads

$$E_{\text{sp}}^{\text{Hx}} = \sum_{i,j}^{N_0/2}\langle ij||ij\rangle + \sum_i^{N_0/2}\langle 0i||0i\rangle, \quad (24)$$

where we introduced the anti-symmetrized integral $\langle ij||kl\rangle = \int d\mathbf{r}d\mathbf{r}'\varphi_i^*(\mathbf{r})\varphi_j^*(\mathbf{r}')v(\mathbf{r}, \mathbf{r}')(2\varphi_k(\mathbf{r})\varphi_l(\mathbf{r}') - \varphi_l(\mathbf{r})\varphi_k(\mathbf{r}'))$. The second term accounts for all interactions of the singly occupied atomic orbital φ_0. The expression for the spin compensated case reads

$$E_{\text{sc}}^{\text{Hx}} = E_{\text{sp}}^{\text{Hx}} + \frac{1}{4}\int d\mathbf{r}d\mathbf{r}'|\varphi_0(\mathbf{r})|^2 v(\mathbf{r}, \mathbf{r}')|\varphi_0(\mathbf{r}')|^2. \quad (25)$$

The additional term is a non-zero self-interaction term, which is equal to the fractional spin error of EXX. It is this term alone that is responsible for the wrong dissociation limit of EXX for H_2. It also introduces a large additional error in the dissociation limit of any system, on top of the error inherent in the EXX functional when describing the fragments.

We now turn to the RPA correlation energy. The correlation energy for the sc system is taken from Eq. (23) with $p = 1$,

$$E_{sc}^c = -\frac{1}{4} \int d\mathbf{r} d\mathbf{r}' |\varphi_0(\mathbf{r})|^2 v(\mathbf{r}, \mathbf{r}') |\varphi_0(\mathbf{r}')|^2$$
$$+ \frac{i}{2} \int_0^1 d\lambda \int_{-\infty}^{\infty} \frac{d\omega}{2\pi} \operatorname{Tr} \left\{ v \left[\tilde{\chi}_\lambda^1(\omega) - \tilde{\chi}_s^1(\omega) \right] \right\}. \quad (26)$$

We now see that the first term exactly cancels the fractional spin error of EXX. The second term in Eq. (23) is identical to the correlation energy obtained in the spin-polarized case. Consequently, the RPA functional does not suffer from fractional spin error. There will, however, still be a self-correlation due to the second term but this is, in general, expected to be smaller. These conclusions are confirmed by the numerical results obtained previously[24–26] and here in Sec. V.

IV. COMPUTATIONAL DETAILS

Our goal is to find the local potential that minimizes the RPA energy functional. For the three-dimensional (3D) calculations, we utilize the direct minimization scheme for the optimized effective potential (OEP) proposed by Yang and Wu.[45] The potential is expanded in a basis plus a reference potential,

$$v(\mathbf{r}) = v_0(\mathbf{r}) + \sum_t b_t g_t(\mathbf{r}). \quad (27)$$

As a reference potential we use the sum of the nuclear potential and the Fermi-Amaldi potential, $v^{FA}(\mathbf{r})$, evaluated with the Hartree-Fock density,

$$v^{FA}(\mathbf{r}) = \frac{N-1}{N} \int \frac{n(\mathbf{r}')}{|\mathbf{r} - \mathbf{r}'|} d\mathbf{r}'. \quad (28)$$

For closed-shell systems, the derivative of the total energy functional with respect to the expansion coefficients, b_t, is readily evaluated via Eq. (4). For systems with fractional charge, we evaluated the gradient with the finite difference method. The gradient is then fed to the Broyden-Fletcher-Goldfarb-Shanno optimization routine to find the minimum total energy. The calculations were considered converged when the vector norm of the gradient was less than 10^{-3}. The algorithm was implemented in a local version of the PyQuante module.[46]

It is a well-known fact that the finite basis set OEP calculations can become numerically unstable if a too large potential basis set is used.[47–49] We carefully chose the potential basis sets to be balanced to the respective orbital basis sets. The proper choice is reflected in the smooth potentials that we obtain. For our calculations, we used the standard orbital basis cc-pVTZ from the Dunning family.

For the potential bases, we used even tempered gaussians. Each set is characterized by three numbers: the smallest exponent, $\alpha_{\min}$, the largest exponent, $\alpha_{\max}$, and the number of

TABLE I. Energies in Hartree.

| Atom | This work | | Benchmark | |
	IP	Energy	IP	Energy
He	−0.907	−2.936	−0.902	−2.945
Be	−0.349	−14.681	−0.354	−14.754
Ne	−0.773	−128.945	−0.796	−129.103

basis functions, N. With this set of parameters, we construct the exponent α_i as

$$\alpha_i = \alpha_{\min} \left[\frac{\alpha_{\max}}{\alpha_{\min}} \right]^{\left(\frac{i-1}{N-1} \right)}, \quad (29)$$

where i runs from 1 to N. For the atomic calculations, we use only s-type functions. For molecular calculations, we add a set of p-type functions using the same exponents and omitting the largest.

For the one-dimensional (1D) calculations, we use a basis set of cubic splines, which permits us to solve Eq. (5) by inverting the static KS response function. The spline-basis is described in detail in several previous works where it has been used successfully for OEP-type of equations.[37,50,51]

V. RESULTS

As a first step, we verify our implementation. To this end, we compare the total energy and the correlation potential with accurate reference data for He, Be, and Ne.[38] The total energies and ionization potentials (IP) are listed in Table I. The potential basis sets are given by $\alpha_{\min} = 0.01$, $\alpha_{\max} = 10$, and $N = 5$ for He, $\alpha_{\min} = 0.01$, $\alpha_{\max} = 10$, and $N = 9$ for Be, and $\alpha_{\min} = 0.001$, $\alpha_{\max} = 100$, and $N = 11$ for Ne (compare Eq. (29)).

The total energies of our new implementation are somewhat higher than the reference energies. The differences range from 9 mH to 158 mH. This result is expected since the reference calculations were performed with a virtually complete orbital basis. The differences in IP are minor (from 5 mH to 23 mH), thus indicating an accurate potential. This conclusion is supported by Figs. 1–3, which show our RPA correlation potentials (dashed) of He, Be, and Ne comparing to the accurate RPA correlation potentials (dotted).[38] The RPA correlation potentials shown in the figures are calculated as

$$v_c^{RPA}(\mathbf{r}) = v_{KS}^{RPA}[n_{RPA}](\mathbf{r}) - v_{KS}^{EXX}[n_{EXX}](\mathbf{r}). \quad (30)$$

In all figures, we qualitatively reproduce the reference potentials. The largest deviation is found close to the nucleus (the x-axis is on a logarithmic scale). For comparison, we also show the exact KS correlation potential (solid)[52] and we see that the RPA correlation potential closely resembles the exact correlation potential.

To analyze the RPA molecular correlation potential, we first investigate a 1D model system with soft Coulomb interactions. The nuclear potentials are $-Z/\sqrt{(x \pm R/2)^2 + 1}$, where Z is the nuclear charge and R is the internuclear distance. The electron-electron interaction is set to $1/\sqrt{(x_1 - x_2)^2 + 1}$. The first system consists of two H atoms
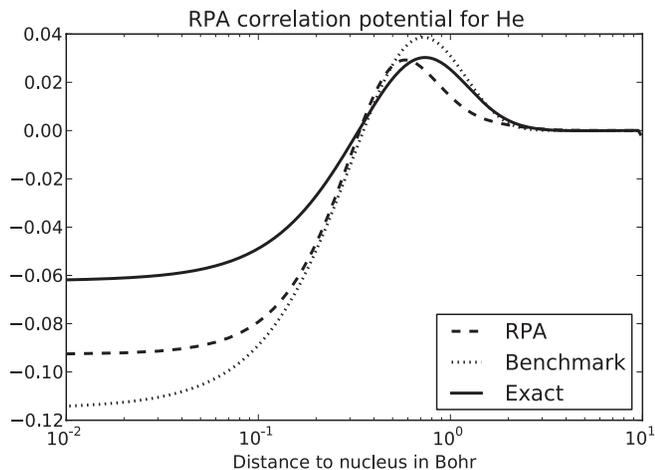
FIG. 1. The correlation potential of He for RPA (Ref. [38]) (dotted), for RPA in this work (dashed), and the exact correlation potential[52] (solid).
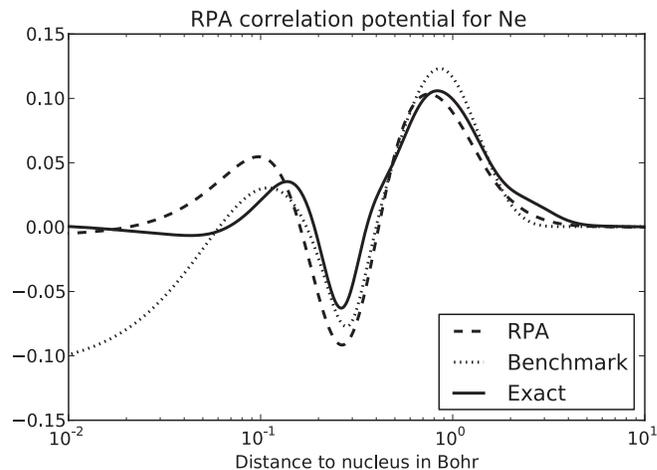

FIG. 3. The correlation potential of Ne for RPA (Ref. [38]) (dotted), for RPA in this work (dashed), and the exact correlation potential[52] (solid).

($Z = 1.2$). Figure 4 shows the RPA correlation potentials along the bond axis at bond distances of 2, 4, and 6 bohrs, with the bond midpoint at zero. We notice that the minimum of the correlation potential is shifted away from the atom, but that the shift decreases with increasing interatomic distance. At the bond midpoint, a positive peak emerges with increasing bond distance. Both features are also observed for the exact KS correlation potential.[31,33]

With our new implementation, we are able to investigate the H$_2$ molecule in all three dimensions and with the full Coulomb interaction (potential basis: $\alpha_{min} = 0.1$, $\alpha_{max} = 1.0$, and $N = 5$). In Figure 5, we show the RPA correlation potential (see Eq. (30)) along the bond axis, where again the bond midpoint is at zero. We show the potentials for equilibrium distance (1.4 bohrs; solid curve), 5.0 bohrs (dotted), and 10.0 bohrs (dashed). The potentials qualitatively resemble the potentials obtained from the 1D calculations (cf. Figure 4). Only the peak at the bond midpoint is absent for small (1.4) and large (10.0) interatomic separations. For large separation, the absence is easily explained. The orbital and potential

basis functions are simply not diffuse enough to extend to the bond midpoint. This results in a vanishing correlation potential at the bond midpoint. The situation is different for a bond distance of 1.4 bohrs. With a small atomic separation, the orbital and potential basis extend to the bond midpoint as is evident from the non-vanishing correlation potential. However, the potential basis functions are not compact enough to produce a peak. We have verified this by using more compact potential basis functions. With this set of basis functions, however, we find unphysical oscillations for larger atomic separations. We also placed orbital and potential functions at various points along the bond axis. We observed a peak in the potential at each of the points, which leads us to conclude that these peaks are artifacts of the basis rather than genuine features of the functional.

At this point, we restrain from showing the dissociation curve and rather point the reader to a future publication with a detailed discussion of the dissociation curves. We would only like to mention that the well-known "bump"[24–27] is still present, but somewhat weaker.
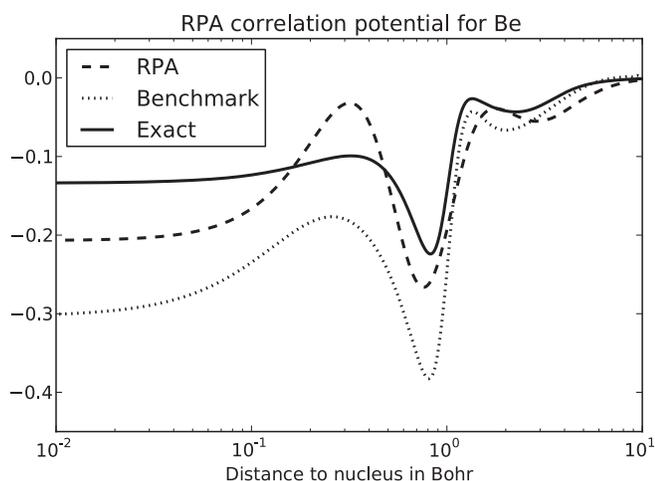

FIG. 2. The correlation potential of Be for RPA (Ref. [38]) (dotted), for RPA in this work (dashed), and the exact correlation potential[52] (solid).
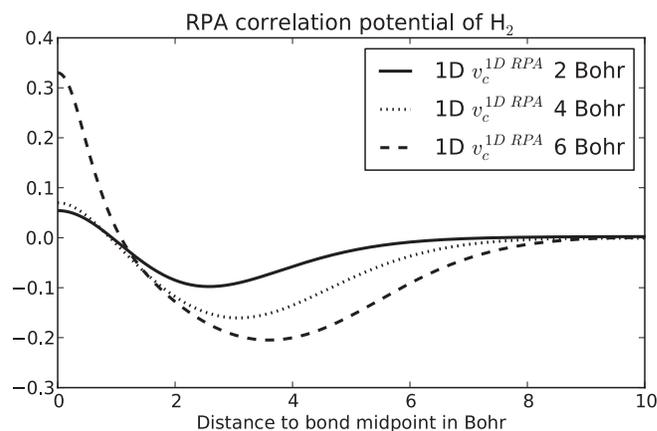

FIG. 4. The correlation potential along the bond axis with the bond midpoint at zero. The system is 1D H$_2$ with a soft Coulomb potential.
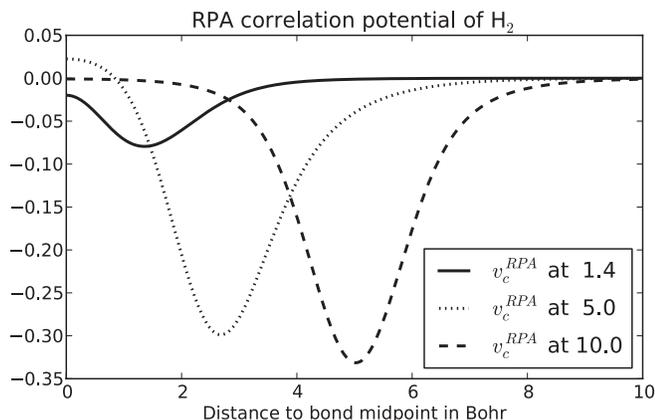
FIG. 5. The correlation potential of H_2 along the bond axis. The bond midpoint is at zero. We show the RPA correlation potential for interatomic distance 1.4 (solid), 5.0 (dotted), and 10.0 (dashed).

FIG. 7. The correlation potential of LiH along the bond axis. The bond midpoint is at zero. The Li atom is located at -1.5, -2.5, and -4 bohrs, respectively. The H atom is located at 1.5, 2.5, and 4 bohrs, respectively.

We now turn to the LiH molecule. In Figure 6, we show the RPA correlation potential (defined in Eq. (30)) of 1D LiH ($Z_{Li} = 3.6$, $Z_H = 1.2$). The solid, dotted, and dashed curves represent the correlation potentials for 2, 3, and 8 bohrs interatomic distances, respectively. The build up of the peak at the bond midpoint is apparent. However, a step, as is present in the exact KS correlation potential, is not observed.

Figure 7 shows the correlation potential (Eq. (30)) of the three-dimensional LiH for bond distances 3 (solid), 6 (dotted), and 8 bohrs (dashed). The parameters for the potential basis of the H atom are $\alpha_{min} = 0.01$, $\alpha_{max} = 1.0$, and $N = 2$. For the Li atom, they read $\alpha_{min} = 0.001$, $\alpha_{max} = 10$, and $N = 3$. The same features as in the 1D case are also found in the results for the 3D correlation potentials. In the region of the Li atom (-10 to 0), the potential qualitatively resembles that of the 1D system in Figure 6. We see a well with a peak close to the nucleus. Also in the region of the H atom (0 to 10) Figures 6 and 7 show the same structure. A well emerges with increasing bond distance. The difference between 1D and 3D

is found only at the bond midpoint. As in the case of H_2, a peak emerges only for the 1D system (Figure 6). In contrast, the 3D system (Figure 7) exhibits a peak at zero only for small and intermediate bond distances (3 and 5 bohrs). The explanation for the absence of the peak at the bond midpoint for 8 bohrs is the same as in the case of H_2.

We further analyze the RPA functional in the context of fractional charge. The total energy of H and Li (potential bases such as in LiH) is plotted (Figures 8 and 9) as a function of the number of electrons, where we allow fractional values, according to Eq. (23). Both atoms show a smooth behavior, thus showing that the RPA (red) misses the kink at integer electron numbers. Comparing to the exact curves, we see, however, a large improvement compared to the EXX (blue) functional regarding the total energy. The agreement is particularly well at integer number of electrons. This explains the good dissociation energies for homoatomic systems found in the RPA. We can also combine these two figures to analyze the RPA energy of LiH in the dissociation limit. In order to do this, we add the energies for the H atom to the energies of the Li atom so that the total number of electrons sums up
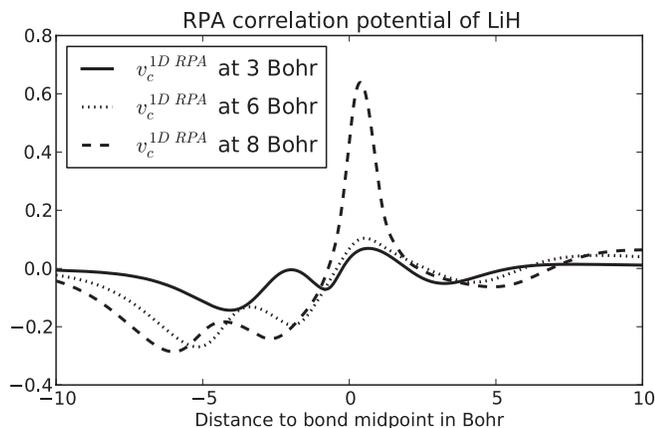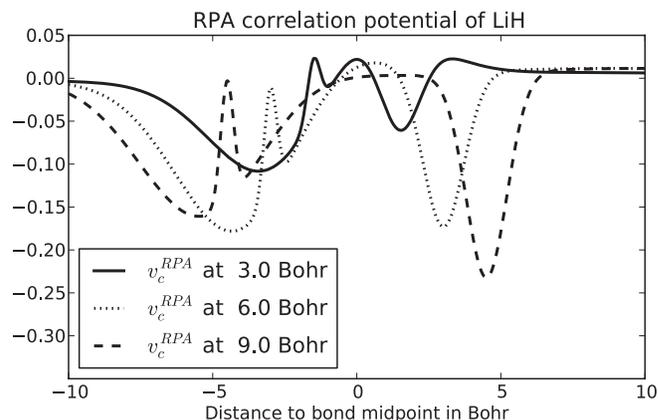

FIG. 6. The correlation potential along the bond with the bond midpoint at zero. The system is 1D LiH with a soft Coulomb potential. The Li atom is located at -1, -1.5, and -4 bohrs, respectively. The H atom is located at 1, 1.5, and 4 bohrs, respectively.
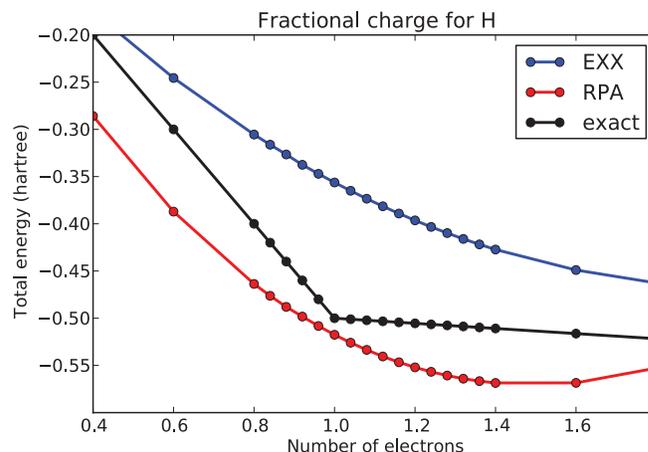

FIG. 8. The total energy of H as a function of number of electrons for EXX (blue), RPA (red), and exact (black).
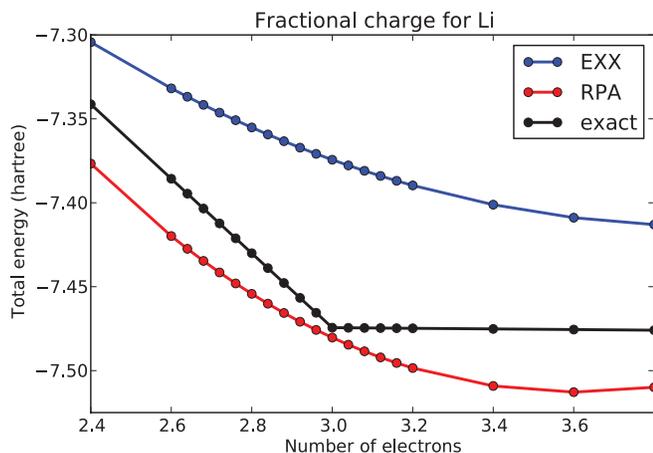
FIG. 9. The total energy of Li as a function of number of electrons for EXX (blue), RPA (red), and exact (black).

TABLE II. Total energies in Hartree in the dissociation limit.

	Exact	EXX	RPA
H_2	-1.000	-0.713	-1.035
Li_2	-14.948	-14.749	-14.961
LiH	-7.974	-7.759	-8.007

to four. Figure 10 shows the total energy as a function of the number of electrons at the H atom. The number of electrons at the Li atom will then be four minus the x value. The exact functional (black) has a minimum at 1.0 because it dissociates LiH into a neutral H atom and a neutral Li atom. In Figure 10, we see that EXX (blue) and RPA (red) do not dissociate LiH into the neutral atoms. In both cases, there is a surplus of electronic charge at the H atom. However, in the case of RPA the surplus (0.16 electrons) is much smaller than in the case of EXX (0.4 electrons). The large improvement may be related to the peak that is present in the RPA correlation potential. Finally, in Table II we collect the total energies in the dissociation limit of H_2, Li_2, and LiH for the exact functional, EXX, and RPA. Please note that the LiH energies of EXX and RPA are taken as the minimum of the respective curves in Figure 10 and not the values at 1.0. This is to account for the fractional charge error present in both functionals.
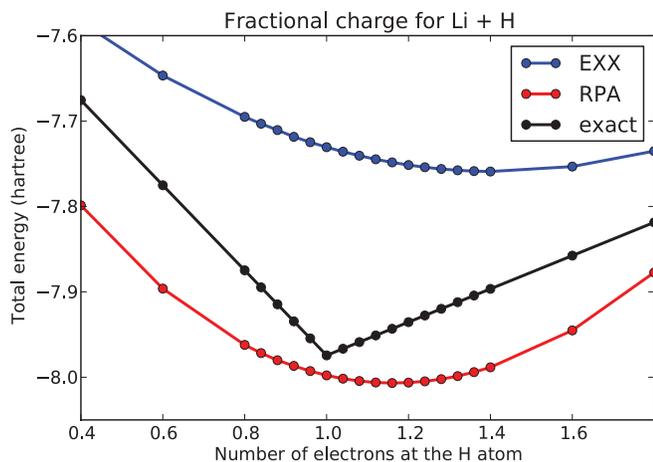
VI. CONCLUSIONS

We have obtained the self-consistent RPA correlation potentials for diatomic molecules and studied their behavior as a function of interatomic distances. At large distances, the RPA potential correctly exhibits a peak at the bond midpoint but misses the step feature.

We have also analyzed the RPA functional for fractional charges by evaluating the ensemble-averaged KS Green function using spin-compensated ensembles with non-integer number of particles. This procedure can be carried over to other functionals constructed from the KS Green function.

The numerical results show that the kink at integer number of electrons is missed in the RPA. As a consequence, we find spurious fractional charges on the dissociated fragments. The charges are, however, much smaller compared to other functionals. On the other hand, the RPA will most likely not be able to describe the so-called field counteracting effect in the correlation potential of hydrogen chains which has been discussed to have its origin in the derivative discontinuity.[53]

In summary, we have found that the RPA accomplishes the following:

- The dissociation limit of closed-shell molecules is well reproduced in the RPA due to the explicit elimination of the self-interaction term present in the EXX functional.
- RPA separates the charges in bond dissociation by virtue of a peak at the bond midpoint, an exact feature of the true correlation potential.
- RPA exhibits only a small fractional charge error in the cases of closed-shell covalently bonded molecules.

These findings consolidate the high expectations on the RPA that are currently prevalent. There is, however, still room for improvement as the discontinuity at odd integer particle number is missing. We believe that improvements on the RPA within the ACFD framework will help to overcome this shortcoming.

APPENDIX: DERIVATIVE OF THE RPA ENERGY

In this Appendix, we return to Eq. (5) and evaluate $n_c(\mathbf{r})$ in terms of KS orbitals, φ_k, and KS eigenvalues, ε_k. The self-energy (Eq. (6)) involves an integration over the frequency of the following form:

$$\Sigma_c(\omega) = i \int \frac{d\omega'}{2\pi} G_s(\omega' + \omega) v \chi^{\mathrm{RPA}}(\omega') v, \qquad (A1)$$

where we have suppressed the space-coordinates. To perform the integration, we write the KS Green function in its

FIG. 10. The total energy of dissociated LiH as a function of number of electrons at the H atom for EXX (blue), RPA (red), and exact (black).

Lehmann representation,

$$G_s(\mathbf{r}, \mathbf{r}', \omega) = \sum_k \varphi_k(\mathbf{r})\varphi_k(\mathbf{r}')$$

$$\times \left[\frac{n_k}{\omega - \varepsilon_k - i\eta} + \frac{1 - n_k}{\omega - \varepsilon_k + i\eta} \right], \quad (A2)$$

where n_k is the occupation number. The response function in the RPA is given by Eq. (7). This equation can easily be rewritten as an eigenvalue problem in terms of the matrix

$$V_{qq'} = \omega_q^2 \delta_{qq'} + \langle \tilde{f}_q | v | \tilde{f}_{q'} \rangle, \quad (A3)$$

where $\tilde{f}_q(\mathbf{r}) = 2\sqrt{\omega_q} f_q(\mathbf{r})$, with $f_q(\mathbf{r})$ being a KS excitation function and ω_q the KS excitation energy. The square root of the eigenvalues corresponds to the true excitation energies Z_q, and the excitation functions are transformed according to

$$F_q(\mathbf{r}) = \sum_{q'} f_{q'}(\mathbf{r}) U_{q'q}, \quad (A4)$$

where U is the matrix diagonalizing V. The interacting time-ordered response function in the RPA can then be written as

$$\chi^{\mathrm{RPA}}(\mathbf{r}, \mathbf{r}', \omega) = \sum_q \frac{1}{2Z_q} F_q(\mathbf{r}) F_q(\mathbf{r}')$$

$$\times \left[\frac{1}{\omega - Z_q + i\eta} - \frac{1}{\omega + Z_q - i\eta} \right], \quad (A5)$$

and the integral in Eq. (A1) becomes

$$\Sigma_c(\mathbf{r}, \mathbf{r}', \omega) = \sum_{kq} \varphi_k(\mathbf{r}) \int d\mathbf{r}_1 v(\mathbf{r}, \mathbf{r}_1) F_q(\mathbf{r}_1)$$

$$\times \varphi_k(\mathbf{r}') \int d\mathbf{r}_1 v(\mathbf{r}', \mathbf{r}_1) F_q(\mathbf{r}_1)$$

$$\times \frac{1}{2Z_q} \left[\frac{1 - n_k}{\omega - \varepsilon_k - Z_q + i\eta} + \frac{n_k}{\omega - \varepsilon_k + Z_q - i\eta} \right]. \quad (A6)$$

Next, we evaluate

$$n_c = -i \int \frac{d\omega}{2\pi} \Sigma_c(\omega) G_s(\omega) G_s(\omega). \quad (A7)$$

After performing standard contour integrations, we get in total six terms, which after symmetry considerations can be reduced to four. In summary, we find

$$n_c(\mathbf{r}) = \sum_{ksp} \sum_q \frac{1}{Z_q} (\ldots) \varphi_s^*(\mathbf{r}) \varphi_p(\mathbf{r})$$

$$\times \int d\mathbf{r}_1 d\mathbf{r}_2 F_q(\mathbf{r}_1) v(\mathbf{r}_1, \mathbf{r}_2) \varphi_k(\mathbf{r}_2) \varphi_p^*(\mathbf{r}_2)$$

$$\times \int d\mathbf{r}_1 d\mathbf{r}_2 \varphi_s(\mathbf{r}_1) \varphi_k^*(\mathbf{r}_1) v(\mathbf{r}_1, \mathbf{r}_2) F_q^*(\mathbf{r}_2), \quad (A8)$$

where the dots signify the insertion of the following four terms:

$$- \frac{(1 - n_k) n_p n_s}{(\varepsilon_k + Z_q - \varepsilon_p)(\varepsilon_k + Z_q - \varepsilon_s)}, \quad (A9)$$

$$+ \frac{2(1 - n_k) n_p (1 - n_s)}{(\varepsilon_p - Z_q - \varepsilon_k)(\varepsilon_p - \varepsilon_s)}, \quad (A10)$$

$$+ \frac{2 n_k n_p (1 - n_s)}{(\varepsilon_s + Z_q - \varepsilon_k)(\varepsilon_p - \varepsilon_s)}, \quad (A11)$$

$$+ \frac{n_k (1 - n_s)(1 - n_p)}{(\varepsilon_s + Z_q - \varepsilon_k)(\varepsilon_p + Z_q - \varepsilon_k)}. \quad (A12)$$

The expression in Eq. (A8) has, in this work, been implemented both in the 3D and in the 1D cases.

[1] F. Furche, Phys. Rev. B **64**, 195120 (2001).
[2] F. Furche, J. Chem. Phys. **129**, 114105 (2008).
[3] H. Eshuis, J. Yarkony, and F. Furche, J. Chem. Phys. **129**, 234114 (2010).
[4] L. Schimka, J. Harl, A. Stroppa, A. Grneis, M. Marsman, F. Mittendorfer, and G. Kresse, Nature Mater. **9**, 741 (2010).
[5] S. Lebègue, J. Harl, T. Gould, J. G. Ángyán, G. Kresse, and J. F. Dobson, Phys. Rev. Lett. **105**, 196401 (2010).
[6] J. Harl and G. Kresse, Phys. Rev. Lett. **103**, 056401 (2009).
[7] X. Ren, A. Tkatchenko, P. Rinke, and M. Scheffler, Phys. Rev. Lett. **106**, 153003 (2011).
[8] X. Ren, P. Rinke, and M. Scheffler, Phys. Rev. B **80**, 045402 (2009).
[9] R. W. Godby, M. Schlüter, and L. J. Sham, Phys. Rev. B **36**, 6497 (1987).
[10] R. W. Godby, M. Schlüter, and L. J. Sham, Phys. Rev. Lett. **56**, 2415 (1986).
[11] M. Grüning, A. Marini, and A. Rubio, J. Chem. Phys. **124**, 154108 (2006).
[12] A. L. Fetter and J. D. Walecka, *Quantum Theory of Many-Particle Systems*, 2nd ed. (Dover, New York, 2003).
[13] F. Aryasetiawan, T. Miyake, and K. Terakura, Phys. Rev. Lett. **88**, 166401 (2002).
[14] M. Fuchs and X. Gonze, Phys. Rev. B **65**, 235109 (2002).
[15] W. Kohn, Y. Meir, and D. E. Makarov, Phys. Rev. Lett. **80**, 4153 (1998).
[16] J. Toulouse, I. C. Gerber, G. Jansen, A. Savin, and J. G. Ángyán, Phys. Rev. Lett. **102**, 096404 (2009).
[17] J. F. Dobson, in *Topics in Condensed Matter Physics*, edited by M. P. Das (Nova, New York, 1994), e-print arXiv:cond-mat/0311371.
[18] H.-V. Nguyen and G. Galli, J. Chem. Phys. **132**, 044109 (2010).
[19] S. Lebègue, J. Harl, T. Gould, J. G. Ángyán, G. Kresse, and J. F. Dobson, Phys. Rev. Lett. **105**, 196401 (2010).
[20] N. Helbig, I. V. Tokatly, and A. Rubio, J. Chem. Phys. **131**, 224105 (2009).
[21] A. J. Cohen, P. Mori-Sánchez, and W. Yang, J. Chem. Phys. **129**, 121104 (2008).
[22] P. Mori-Sánchez, A. J. Cohen, and W. Yang, Phys. Rev. Lett. **102**, 066403 (2009).
[23] A. J. Cohen, P. Mori-Sánchez, and W. Yang, Science **321**, 792 (2008).
[24] N. E. Dahlen, R. van Leeuwen, and U. von Barth, Int. J. Quantum Chem. **101**, 512 (2005).
[25] M. Fuchs, Y.-M. Niquet, X. Gonze, and K. Burke, J. Chem. Phys. **122**, 094116 (2005).
[26] N. E. Dahlen, R. van Leeuwen, and U. von Barth, Phys. Rev. A **73**, 012511 (2006).
[27] A. Heßelmann and A. Görling, Phys. Rev. Lett. **106**, 093001 (2011).
[28] J. P. Perdew, R. G. Parr, M. Levy, and J. L. Balduz, Phys. Rev. Lett. **49**, 1691 (1982).
[29] P. Mori-Sánchez, A. J. Cohen, and W. Yang, Phys. Rev. Lett. **100**, 146401 (2008).
[30] P. Mori-Sánchez, A. Cohen, and W. Yang, e-print arXiv:0903.4403v1.
[31] O. V. Gritsenko and E. J. Baerends, Phys. Rev. A **54**, 1957 (1996).
[32] P. R.T. Schipper, O. V. Gritsenko, and E. J. Baerends, Phys. Rev. A **57**, 1729 (1998).
[33] D. Tempel, T. J. Martinez, and N. T. Maitra, J. Chem. Theory Comput. **5**, 770 (2009).
[34] J. P. Perdew, in *Density Functional Methods in Physics*, edited by R. M. Dreizler and J. da Providencia (Plenum, New York, 1985).
[35] E. Sagvolden and J. P. Perdew, Phys. Rev. A **77**, 012517 (2008).
[36] M. A. Buijse, E. J. Baerends, and J. G. Snijders, Phys. Rev. A **40**, 4190 (1989).
[37] M. Hellgren and U. von Barth, Phys. Rev. B **76**, 075107 (2007).
[38] M. Hellgren and U. von Barth, J. Chem. Phys. **132**, 044101 (2010).

[39]D. C. Langreth and J. P. Perdew, Solid State Commun. **17**, 1425 (1975).

[40]O. Gunnarsson and B. I. Lundqvist, Phys. Rev. B **13**, 4274 (1976).

[41]*Time-Dependent Density Functional Theory*, edited by M. Marques, C. A. Ullrich, F. Nogueira, A. Rubio, K. Burke, and E. K. U. Gross (Springer, Berlin, 2006).

[42]E. K. U. Gross and W. Kohn, Phys. Rev. Lett. **55**, 2850 (1985).

[43]L. J. Sham and M. Schlüter, Phys. Rev. Lett. **51**, 1888 (1983).

[44]U. von Barth, N. Dahlen, R. van Leeuwen, and G. Stefanucci, Phys. Rev. B **72**, 235109 (2005).

[45]W. Yang and Q. Wu, Phys. Rev. Lett. **89**, 143002 (2002).

[46]See http://pyquante.sourceforge.net/ for the source code and description of the PyQuante module to Python.

[47]D. R. Rohr, O. V. Gritsenko, and E. J. Baerends, Chem. Phys. Lett. **432**, 336 (2006).

[48]D. R. Rohr and A. Savin, J. Mol. Struct. **943**, 90 (2010).

[49]A. Heßelmann, A. W. Götz, F. D. Salla, and A. Görling, J. Chem. Phys. **127**, 054102 (2007).

[50]H. Bachau, E. Cormier, P. Decleva, J. E. Hansen, and F. Martin, Rep. Prog. Phys. **64**, 1815 (2001).

[51]M. Hellgren and U. von Barth, J. Chem. Phys. **131**, 044110 (2009).

[52]C. J. Umrigar and X. Gonze, Phys. Rev. A **50**, 3827 (1994).

[53]S. J. A. van Gisbergen, P. R.T. Schipper, O. V. Gritsenko, E. J. Baerends, J. G. Snijders, B. Champagne, and B. Kirtman, Phys. Rev. Lett. **83**, 694 (1999).